Science Advances
AAAS

Supplementary Materials for

Coupled topological flat and wide bands: Quasiparticle formation and destruction

Haoyu Hu and Qimiao Si

Corresponding author: Qimiao Si, qmsi@rice.edu.

Sci. Adv. **9**, eadg0028 (2023)
DOI: 10.1126/sciadv.adg0028

This PDF file includes:

Supplementary Material

A. Band topology and Wannier construction

The space group is generated by the translational symmetry and the mirror M_x symmetry. At $\gamma = 0$, the model has an additional C_{3z} symmetry. We observe a completely flat band and a quadratic band touching between the flat and wide bands, as shown in Figs. S1B,C. By introducing a non-zero γ, the flat band is no longer completely flat, but its bandwidth remains relatively narrow at small γ. Near Γ there is a linear crossing (Dirac node) between the flat band and wide band as shown in fig. S1D. Such Dirac node is protected by the M_x and $SU(2)$ spin symmetry. If we introduce spin-orbit coupling that breaks the $SU(2)$ spin symmetry, the Dirac node will be gapped out and the flat band acquires ± 1 Chern number. In fig. S1E, we show the band structure of the following spin-orbit coupling

$$H_{soc} = \sum_{\boldsymbol{k},\sigma} i\lambda\sigma \left[\eta^{\dagger}_{\boldsymbol{k},C,\sigma}\eta_{\boldsymbol{k},D,\sigma} + \eta^{\dagger}_{\boldsymbol{k},D,\sigma}\eta_{\boldsymbol{k},E,\sigma} + \eta^{\dagger}_{\boldsymbol{k},E,\sigma}\eta_{\boldsymbol{k},C,\sigma} \right] + \text{h.c.} \tag{S1}$$

We can also observe the non-trivial topology by calculating the M_x eigenvalue of each band at high symmetry points, where $\eta^{\dagger}$ creates an electron with the d_{z^2} orbital that is even under M_x transformation. We focus on the case of $\gamma \neq 0$ and show the result in table S1 and also in fig. S1D,E. We note that, at $\gamma \neq 0$, each band forms a one-dimensional (1d) irreducible representation of the little group at each high-symmetry point, which is characterized by the M_x eigenvalue. However, in the case of $\gamma = 0$, we have both C_{3z} and M_x symmetries, and therefore, a two-dimensional (2d) irreducible representation could be formed by the bands at high symmetry points. The case of $\gamma \neq 0$ simplifies the construction of the Wannier orbitals but still keeps the non-trivial topology of the band structure. At $\gamma \neq 0$, the flat band is non-longer perfectly flat. However, as long as $|\gamma| \lesssim 0.2t$, the middle bands still remain relatively flat and the consideration of Wannier construction in this section still holds.

The high symmetry points are $\Gamma = (0,0), M' = (2\pi/\sqrt{3}, 0), K = (0, 4\pi/3)$ and we label

the bands from the top to the bottom as band $1, 2, 3, 4, 5$, with band 3 being the flat band. We note that a non-zero but small λ will not change the M_x eigenvalue of each band. If we only consider the flat band (band 3), its M_x eigenvalues at Γ, M, K are $-1, +1, +1$ respectively, which do not admit a Wannier-orbital representation that preserves all the symmetry. However, by taking band 2 at the Γ point and band 3 at the M' and K points, we have the M_x eigenvalue $+1, +1, +1$ which can be represented by an M_x-even Wannier orbital. This indicates that we can construct the Wannier orbitals by combining bands 2 and 3. A related procedure has been taken for moiré systems (*38*). As we show later, the constructed Wannier orbital would have a large overlap with the flat band and can be used to represent the flat-band degrees of freedom. After removing the $+1, +1, +1$ eigenvalues at Γ, M', K, the remaining eigenvalues are $+1, -1$ for Γ point, $+1, -1$ for M' point and $+1, -1$ for K point. These combinations admit two Wannier orbitals that are mirror even and mirror odd respectively. These two Wannier orbitals mainly describe wide-band degrees of freedom.

We now construct the Wannier orbitals for the case of $\gamma = -0.1, \lambda = 0$. However, the same procedure applies to the case with a small but non-zero λ. We introduce the following three trial wavefunctions (six trial wavefunctions if we account for the spin degeneracy) and construct the Wannier orbitals of the top three bands via the projection method:

$$|\text{Trial}; d, \boldsymbol{R}, \sigma\rangle = \sum_{\boldsymbol{r},i} e^{-\frac{(\boldsymbol{r}-\boldsymbol{R})^2}{2r_0^2}} \alpha_i^f \eta_{\boldsymbol{r},i,\sigma}|0\rangle$$

$$|\text{Trial}; c, 1, \boldsymbol{R}, \sigma\rangle = \sum_{\boldsymbol{r},i} e^{-\frac{(\boldsymbol{r}-\boldsymbol{R})^2}{2r_0^2}} r_x \eta_{\boldsymbol{r},i,\sigma}|0\rangle$$

$$|\text{Trial}; c, 2, \boldsymbol{R}, \sigma\rangle = \sum_{\boldsymbol{r},i} e^{-\frac{(\boldsymbol{r}-\boldsymbol{R})^2}{2r_0^2}} r_y \eta_{\boldsymbol{r},i,\sigma}|0\rangle$$

where $r_0 = 0.25a_0$, with a_0 being the distance between the two nearest atoms, describes the decaying rate. $\alpha^d_{A,B,C,D,E} (= 0.5, 0.5, 1.4, 1, 1)$ captures the imbalance of weight distributions between different sublattices. After the projection procedure, we find three exponentially-

localized Wannier orbitals $|d, \boldsymbol{R}, \sigma\rangle, |c, \boldsymbol{R}, 1, \sigma\rangle, |c, \boldsymbol{R}, 2, \sigma\rangle$, which come from the three trial wavefunctions respectively. We then define the electron operators in the Wannier basis via

$$d^\dagger_{\boldsymbol{R},\sigma}|0\rangle = |d, \boldsymbol{R}, \sigma\rangle \quad , \quad c^\dagger_{\boldsymbol{R},1,\sigma}|0\rangle = |c, \boldsymbol{R}, 1, \sigma\rangle \quad , \quad c^\dagger_{\boldsymbol{R},2,\sigma}|0\rangle = |c, \boldsymbol{R}, 2, \sigma\rangle \, .$$

By construction, both $d_{\boldsymbol{R},\sigma}$ and $c_{\boldsymbol{R},2,\sigma}$ are even under M_x and $c_{\boldsymbol{R},1,\sigma}$ is odd under M_x.

In addition, we also calculate the orbital weight of each band, which characterizes the overlapping between each band and each Wannier orbital. The overlappings between the Wannier orbitals $d_{\boldsymbol{k},\sigma}, c_{\boldsymbol{k},1,\sigma}$ and $c_{\boldsymbol{k},2,\sigma}$ and the i-th band are defined as

$$\begin{aligned}
W_i^d &= \frac{1}{2N}\sum_{\boldsymbol{k}}\sum_{\sigma} |\langle u_{\boldsymbol{k},i,\sigma}|d, \boldsymbol{k}, \sigma\rangle|^2 \\
W_i^{c,1} &= \frac{1}{2N}\sum_{\boldsymbol{k}}\sum_{\sigma} |\langle u_{\boldsymbol{k},i,\sigma}|c, \boldsymbol{k}, 1, \sigma\rangle|^2 \\
W_i^{c,2} &= \frac{1}{2N}\sum_{\boldsymbol{k}}\sum_{\sigma} |\langle u_{\boldsymbol{k},i,\sigma}|c, \boldsymbol{k}, 2, \sigma\rangle|^2
\end{aligned}$$

where $|u_{\boldsymbol{k},i,\sigma}\rangle$ is the Bloch function of the i-th band with spin index σ, $|d, \boldsymbol{k}, \sigma, \rangle, |c, \boldsymbol{k}, 1, \sigma\rangle, |c, \boldsymbol{k}, 2, \sigma\rangle$ are the Fourier transformation of $|d, \boldsymbol{R}, \sigma\rangle, |c, \boldsymbol{R}, 1, \sigma\rangle, |c, \boldsymbol{R}, 2, \sigma\rangle$ respectively. Because of the $SU(2)$ spin symmetry, we average over the contributions between the spin up and spin down. From numerical calculations, we have

$$\begin{aligned}
&W_1^d = 0\% \quad , \quad W_2^d = 12\% \quad , \quad W_3^d = 88\% \quad , \quad W_4^d = 0\% \quad , \quad W_5^d = 0\% \\
&W_1^{c,1} = 34\% \quad , \quad W_2^{c,1} = 57\% \quad , \quad W_3^{c,1} = 9\% \quad , \quad W_4^{c,1} = 0\% \quad , \quad W_5^{c,1} = 0\% \\
&W_1^{c,2} = 66\% \quad , \quad W_2^{c,2} = 31\% \quad , \quad W_3^{c,2} = 3\% \quad , \quad W_4^{c,2} = 0\% \quad , \quad W_5^{c,2} = 0\%
\end{aligned}$$

where we label the bands from the top to the bottom as $1, 2, 3, 4, 5$; band 3 is the flat band. We observe that the flat bands are mainly represented by the d orbitals, and the two dispersive bands (1 and 2) are mainly captured by the two c orbitals.

Our Wannier construction equally applies for the case with spin-orbit coupling. By implementing the same trial state as described in Eq. S2, we are able to construct exponentially-

localized Wannier orbitals without breaking any symmetry of the Hamiltonian. The resulting Wannier function at relatively small but still sizeable spin-orbit coupling $(\lambda/t = 0.05)$ is adiabatically connected to the Wannier functions at zero spin-orbit coupling. Similarly as for the case without spin-orbit coupling, we observe that the flat bands are mainly represented by the d orbitals, and the two dispersive bands (1 and 2) are mainly captured by the two c orbitals. The corresponding orbital weights are listed below.

$$
\begin{aligned}
&W_1^d = 0\% \quad , \quad W_2^d = 12\% \quad , \quad W_3^d = 88\% \quad , \quad W_4^d = 0\% \quad , \quad W_5^d = 0\% \\
&W_1^{c,1} = 35\% \quad , \quad W_2^{c,1} = 57\% \quad , \quad W_3^{c,1} = 8\% \quad , \quad W_4^{c,1} = 0\% \quad , \quad W_5^{c,1} = 0\% \\
&W_1^{c,2} = 65\% \quad , \quad W_2^{c,2} = 31\% \quad , \quad W_3^{c,2} = 4\% \quad , \quad W_4^{c,2} = 0\% \quad , \quad W_5^{c,2} = 0\%
\end{aligned}
\tag{S2}
$$

where we observe, even with the nonzero spin-orbit coupling, the flat band can still be faithfully represented by a localized d electron operators (where the overlapping between flat band and d electron operator is 88%. In fig. S2, we plot the decaying of the Wannier functions of d electrons for both cases of zero and nonzero spin-orbit coupling (SOC). We observe that, in both cases, the Wannier functions are well localized and decay exponentially. Moreover, the Wannier functions in two cases share the similar decaying patterns since a nonzero but small SOC only leads to a small change to the Wannier function.

For this work, we will focus on the model without spin-orbit coupling to simplify the calculations. However, we mention that, our results apply to the case with nonzero SOC. Even though the nonzero SOC breaks the SU(2) symmetry, phases and critical points remain robust against a nonzero but small SOC. The stability of the different phases is seen as follows. For the Kondo or heavy-Fermi-liquid phase, the small SU(2) breaking is irrelevant in the renormalization group sense and the Kondo physics has been observed experimentally and theoretically in various different systems without SU(2) symmetry (*49*). For the Kondo-destroyed phases and

Kondo destruction quantum critical point, it has been demonstrated via both the renormalization group and quantum Monte Carlo methods that both could be stabilized in the cases without an SU(2) symmetry (*46, 47, 49*).

B. Parameters of the model

After constructing the Wannier orbitals, we project the hopping and interaction terms to the Wannier basis, which leads to an interacting model. In this section, we provide the parameters of the interacting model. The parameters of the hopping and hybridization are shown in table. S2. We also determine the dominant local interactions as follows,

$$u/U = 0.149 \quad , \quad F_1/U = 0.044 \quad , \quad F_2/U = 0.036 \quad , \quad J_1/U = 0.088 \quad , \quad J_2/U = 0.072 \tag{S3}$$

Here, the pairing hopping terms (*i.e.* $d^\dagger d^\dagger cc, c^\dagger c^\dagger dd$) have negligible effect, because we focus on the interaction range where the Hubbard interaction u turns the d electron into a quantum spin, and are hence dropped. Moreover, the interactions between the c electrons only renormalize the bandwidth of the c electrons, given that the bandwidth of the c electrons is much larger than the interactions in the parameter region we consider; thus, the interactions between the c electrons are also dropped.

C. Effective multi-orbital Hubbard (Anderson-lattice) model

The model, expressed in terms of the d and c orbitals, contains the kinetic term H_0 and the interaction term H_I. The kinetic term takes the following form:

$$\begin{aligned}
H_0 &= H_d + H_c + H_{dc} \\
H_d &= \sum_{\boldsymbol{R},\boldsymbol{R}',\sigma} \left[t^d_{\boldsymbol{R}-\boldsymbol{R}',\sigma} + (E_d - \mu)\delta_{\boldsymbol{R},\boldsymbol{R}'} \right] d^\dagger_{\boldsymbol{R},\sigma} d_{\boldsymbol{R}',\sigma} \\
H_c &= \sum_{\boldsymbol{R},\boldsymbol{R}',a,a',\sigma} \left[t^c_{\boldsymbol{R}-\boldsymbol{R}',aa',\sigma} - \mu\delta_{\boldsymbol{R},\boldsymbol{R}'}\delta_{a,a'} \right] c^\dagger_{\boldsymbol{R},a,\sigma} c_{\boldsymbol{R}',a',\sigma} + \sum_{\boldsymbol{R},a,\sigma} E_a c^\dagger_{\boldsymbol{R},a,\sigma} c_{\boldsymbol{R},a,\sigma} \\
H_{dc} &= \sum_{\boldsymbol{R},\boldsymbol{R}',a,\sigma} \left[V_{\boldsymbol{R}-\boldsymbol{R}',a,\sigma} d^\dagger_{\boldsymbol{R},\sigma} c_{\boldsymbol{R}',a',\sigma} + \text{h.c.} \right] .
\end{aligned} \tag{S4}$$

The dominant hybridization is between $d_{\boldsymbol{R},a,\sigma}$ and the new conduction-electron band 1, $c_{\boldsymbol{R},1,\sigma}$, which is mirror odd; correspondingly, the hybridization is off-site. For interactions, it suffices to keep the ones between two d-electrons and those between the d- and c-electrons. As mentioned earlier, the interactions between the c-electrons are omitted; they are unimportant, being small compared to the corresponding bandwidth.

The interactions include the Hubbard interaction of the d electrons (H_u), the density-density interactions between the d and c electrons (H_F) (which is unimportant in the local-moment regime that we focus on), and the Hund's coupling between the d and c electrons (H_{Hund}). These interactions are labeled by $u, F_{1,2}, J_{1,2}$, respectively. The full interacting part of the Hamiltonian takes the form of

$$\begin{aligned}
&H_I = H_u + H_F + H_{Hund} \\
&H_u = \sum_{\boldsymbol{R}} \frac{u}{2}(n^d_{\boldsymbol{R}} - 1)^2 \quad , \quad H_F = \sum_{\boldsymbol{R},a} F_a n^f_{\boldsymbol{R}} n^c_{\boldsymbol{R},a}, \\
&H_{Hund} = -\sum_{\boldsymbol{R},a} J_a \boldsymbol{S}_{\boldsymbol{R}} \cdot \boldsymbol{S}^c_{\boldsymbol{R},a} \, .
\end{aligned} \tag{S5}$$

Here, $\boldsymbol{S}_{\boldsymbol{R}} = \frac{1}{2} d^\dagger_{\boldsymbol{R}} \boldsymbol{\sigma} d_{\boldsymbol{R}}$ and $\boldsymbol{S}^c_{\boldsymbol{R},a} = \frac{1}{2} c^\dagger_{\boldsymbol{R},a} \boldsymbol{\sigma} c_{\boldsymbol{R},a}$ are the spin operators of the d- and c-electrons,

respectively; $n^d_{\boldsymbol{R},\sigma} = d^\dagger_{\boldsymbol{R},\sigma} d_{\boldsymbol{R},\sigma}$ and $n^c_{\boldsymbol{R},a,\sigma} = c^\dagger_{\boldsymbol{R},a,\sigma} c_{\boldsymbol{R},a,\sigma}$ are the density operators of the d and c electrons, respectively; $n^d_{\boldsymbol{R}} = \sum_\sigma n^d_{\boldsymbol{R},\sigma}, n^c_{\boldsymbol{R},a} = \sum_\sigma n^c_{\boldsymbol{R},a,\sigma}$.

D. Effective Kondo-lattice model

In this section, we derive the low-energy effective model for sufficiently large values of u. The action of the original Hamiltonian reads

$$S = \int_\tau \sum_{\boldsymbol{R},\sigma} d^\dagger_{\boldsymbol{R},\sigma} \partial_\tau d_{\boldsymbol{R},\sigma} + \int_\tau \sum_{\boldsymbol{R},a,\sigma} c^\dagger_{\boldsymbol{R},a,\sigma} \partial_\tau c_{\boldsymbol{R},a,\sigma} + \int_\tau (H_d + H_c + H_{dc} + H_U + H_F + H_{Hund}) d\tau \,.$$

We perform a Hubbard-Stratonovich transformation to decouple the Hubbard interaction and Hund's coupling term

$$\begin{aligned} Z &= \int_{d,d^\dagger,c,c^\dagger} e^{-S} \\ &= \int_{d,d^\dagger,c,c^\dagger,\phi} \exp\Big\{ - \int_\tau \sum_{\boldsymbol{R},\sigma} d^\dagger_{\boldsymbol{R},\sigma} \partial_\tau d_{\boldsymbol{R},\sigma} - \int_\tau \sum_{\boldsymbol{R},a,\sigma} c^\dagger_{\boldsymbol{R},a,\sigma} \partial_\tau c_{\boldsymbol{R},s,\sigma} - \int_\tau (H_f + H_c + H_{dc} + H_F) \\ &\quad - \int_\tau \sum_{\boldsymbol{R}} \frac{2u}{3} \boldsymbol{\phi}_{\boldsymbol{R}} \cdot \boldsymbol{\phi}_{\boldsymbol{R}} + \int_\tau \frac{4u}{3} \sum_{\boldsymbol{R}} \boldsymbol{\phi}_{\boldsymbol{R}} \cdot (\boldsymbol{S}^d_{\boldsymbol{R}} + \sum_a \frac{3J_a}{4u} \boldsymbol{S}^c_{\boldsymbol{R}a}) \Big\} \end{aligned}$$

where we have dropped the interactions between the conduction electrons. We then introduce the special unitary matrix $U_{\boldsymbol{R}}$ that satisfies

$$\phi_0 U^\dagger_{\boldsymbol{R}} \sigma^z U_{\boldsymbol{R}} = \sum_\mu \phi^\mu_{\boldsymbol{R}} \sigma^\mu \tag{S6}$$

and the new fermions operators

$$\psi_{\boldsymbol{R},\sigma} = \sum_{\sigma'} [U^\dagger_{\boldsymbol{R}}]_{\sigma\sigma'} d_{\boldsymbol{R},\sigma'} \,. \tag{S7}$$

We parametrize $U_{\boldsymbol{R}}$ with

$$U_{\boldsymbol{R}} = \begin{bmatrix} z_{\boldsymbol{R},1} & -z^\dagger_{\boldsymbol{R},2} \\ z_{\boldsymbol{R},2} & z^\dagger_{\boldsymbol{R},1} \end{bmatrix} \tag{S8}$$

with $\sum_a z^\dagger_{\boldsymbol{R},a} z_{\boldsymbol{R},a} = 1$. We then have the following action

$$
\begin{aligned}
S &= S_\psi + S_B + S_t + S_V + S_F + S_c + S_\phi \\
S_\psi &= \int_\tau \sum_{\boldsymbol{R},\sigma} \psi^\dagger_{\boldsymbol{R},\sigma} \partial_\tau \psi_{\boldsymbol{R}\sigma} - \int_\tau \frac{4u}{3} \sum_{\boldsymbol{R}} \phi_0 \psi^\dagger_{\boldsymbol{R}} \sigma^z \psi_{\boldsymbol{R}} \\
S_B &= \int_\tau \sum_{\boldsymbol{R}} \psi^\dagger_{\boldsymbol{R}} (U^\dagger_{\boldsymbol{R}} \partial_\tau U_{\boldsymbol{R}}) \psi_{\boldsymbol{R}} \\
S_t &= \int_\tau \sum_{\boldsymbol{R},\boldsymbol{R}'} t_{\boldsymbol{R},\boldsymbol{R}'} \psi^\dagger_{\boldsymbol{R}} U^\dagger_{\boldsymbol{R}} U_{\boldsymbol{R}'} \psi_{\boldsymbol{R}'} \\
S_V &= \int_\tau \sum_{\boldsymbol{R},\boldsymbol{R}',a} V_{\boldsymbol{R},\boldsymbol{R}'a} \psi^\dagger_{\boldsymbol{R}} U^\dagger_{\boldsymbol{R}} c_{\boldsymbol{R}',a,\sigma} \\
S_c &= \int_\tau \sum_{\boldsymbol{R},a,\sigma} c^\dagger_{\boldsymbol{R},a,\sigma} \partial_\tau c_{\boldsymbol{R},s,\sigma} + \int_\tau \frac{4u}{3} \sum_{\boldsymbol{R}} \phi_0 U^\dagger_{\boldsymbol{R}} \sigma^z U_{\boldsymbol{R}} \cdot (\sum_a \frac{3J_a}{4u} \boldsymbol{S}^c_{\boldsymbol{R}a}) + \int_\tau \sum_{\boldsymbol{R},a} F_a \sum_\sigma \psi^\dagger_{\boldsymbol{R},\sigma} \psi_{\boldsymbol{R},\sigma} n^c_{\boldsymbol{R},c} + H_c \\
S_\phi &= \int_\tau \sum_{\boldsymbol{R}} \frac{2u}{3} \boldsymbol{\phi}_{\boldsymbol{R}} \cdot \boldsymbol{\phi}_{\boldsymbol{R}}
\end{aligned}
$$

The large U leads to a local moment formation, which gives $\phi_0 \neq 0$ at the saddle point level. A non-zero ϕ_0 will then gap out the ψ fermions. We can safely integrate out the gapped ψ fermion, which gives the following new action at the leading order

$$
\begin{aligned}
&S' = S_{Berry} + S_{Heisenberg} + S_{Kondo} + S_c \\
&S_{Berry} = \langle S_B \rangle_0 = -\int_\tau \sum_{\boldsymbol{R},a} z_{\boldsymbol{R},a} \partial_\tau z^\dagger_{\boldsymbol{R},a} \\
&S_{Heisenberg} = -\frac{1}{2} \langle S_t^2 \rangle_0 = \int_\tau \sum_{\boldsymbol{R},\boldsymbol{R}'} \frac{2|t_{\boldsymbol{R},\boldsymbol{R}'}|^2}{4u\phi_0/3} \boldsymbol{S}_{\boldsymbol{R}} \cdot \boldsymbol{S}_{\boldsymbol{R}'} \\
&S_{Kondo} = -\frac{1}{2} \langle S_V^2 \rangle_0 = \int_\tau \sum_{\boldsymbol{R},\boldsymbol{R}_1 a_1,\boldsymbol{R}_2 a_2} \frac{4V^*_{\boldsymbol{R},\boldsymbol{R}_2 a_2} V_{\boldsymbol{R},\boldsymbol{R}_1 a_1}}{4u\phi_0/3} \boldsymbol{S}_{\boldsymbol{R}} \cdot c^\dagger_{\boldsymbol{R},a_1} \boldsymbol{\sigma} c_{\boldsymbol{R},a_2}
\end{aligned}
$$

where for a given operator O, $\langle O \rangle_0 = \left[\int_{\psi,\psi^\dagger} O e^{-S} \right] / \left[\int_{\psi,\psi^\dagger} e^{-S} \right]$ and the spin operator $\boldsymbol{S}_{\boldsymbol{R}}$ is defined as $\boldsymbol{S}_{\boldsymbol{R}} = \frac{1}{2} z^\dagger_{\boldsymbol{R}} \boldsymbol{\sigma} z_{\boldsymbol{R}}$, which is the spin moment of a d electron. S_{Berry} is the Berry phase term of the spin operator $\boldsymbol{S}_{\boldsymbol{R}}$, $S_{Heisenberg}$ and S_{Kondo} are the Heisenberg interaction and Kondo interaction term respectively. Finally, we transform the action to the Hamiltonian and

reach the Kondo-Heisenberg Hamiltonian with the Hund's coupling as shown in the main text.

E. Competition between the Heisenberg/RKKY interactions and Kondo coupling

There are two emergent energy scales in the Kondo lattice model: the Kondo energy scale E_K and the Heisenberg/RKKY scale E_H. The Kondo scale $E_K \sim De^{-1/(\rho J^K)}$, where $J^K = \max\{J^K_{\boldsymbol{R},\boldsymbol{R}_1 a_1,\boldsymbol{R}_2 a_2}\}$ is the maximum amplitude of the Kondo coupling, ρ is the c-electron density of states at the Fermi energy, and D is the bandwidth of the c bands. The Heisenberg/RKKY scale E_H describes the inter-moment interactions, and is proportional to the $J^H = \max\{J^H_{\boldsymbol{R},\boldsymbol{R}'}\}$. When $E_K \gg E_H$, the Kondo physics dominates; the d electrons are Kondo-screened by the c electrons and a heavy Fermi liquid ensues. When $E_H \gg E_K$, the inter-moment exchange interactions prevail. They favor the formation of spin singlets between the d-spins and, thus, are detrimental to the Kondo effect. The competition between the two effects is conveniently captured by tuning $\widetilde{u}$.

We remark that the effective Hund's coupling here is different from the usual atomic cases in an important way. Here, it operates between the localized d-electrons and the wide-band c electrons. Thus, unlike the atomic Hund's coupling, here the Hund's coupling has a very minimal effect on the competition between the inter-moment spin exchange and Kondo coupling. Specifically, in the regime where the inter-d-moment exchange interaction dominates, we can consider the inter-moment spin singlet as being formed from the Hund's coupled effective moment. The latter is primarily made up of the d-spins due to the large c-electron bandwidth. In the Kondo-dominating regime, there is one additional feature that further reduces the effect of the Hund's coupling: The leading Kondo coupling is off-site, in contrast to the onsite nature of the Hund's coupling. Thus, the Hund's coupling likewise will not disturb the formation of the Kondo singlet between the d- and c-spins.

F. Large-N limit

We solve the Kondo-Heisenberg model with the Hund's coupling in a large-N limit. We generalize $SU(2)$ spin symmetry to $SU(N)$ spin symmetry and let $J^H_{\boldsymbol{R},\boldsymbol{R}'} \to J^H_{\boldsymbol{R},\boldsymbol{R}'}/N$ and $J^K_{\boldsymbol{R},\boldsymbol{R}_1 a_1,\boldsymbol{R}_2 a_2} \to J^K_{\boldsymbol{R},\boldsymbol{R}_1 a_1,\boldsymbol{R}_2 a_2}/N, J_a \to J_a/N$. We then introduce Abrikosov fermions $f_{\boldsymbol{R},\sigma}$, which satisfy a local constraint $\sum_\sigma f^\dagger_{\boldsymbol{R},\sigma} f_{\boldsymbol{R},\sigma} = 1$, and rewrite the spin operators as $\boldsymbol{S}_{\boldsymbol{R}} = \frac{1}{2}\sum_{\sigma,\sigma'} f^\dagger_{\boldsymbol{R},\sigma}\boldsymbol{\sigma}_{\sigma,\sigma'} f_{\boldsymbol{R},\sigma'}$.

We next perform a Hubbard-Stratonovich transformation

$$
\begin{aligned}
H_H &\to \sum_{\boldsymbol{R},\boldsymbol{R}'} \frac{J^H_{\boldsymbol{R},\boldsymbol{R}'}}{2}\left[N\chi_{\boldsymbol{R}',\boldsymbol{R}}\chi_{\boldsymbol{R}',\boldsymbol{R}} - \sum_\sigma\left(f^\dagger_{\boldsymbol{R},\sigma} f_{\boldsymbol{R}',\sigma}\chi_{\boldsymbol{R}',\boldsymbol{R}} + \text{h.c.}\right)\right] \\
H_{J_K} &\to \sum_{\boldsymbol{R},\boldsymbol{R}_1,\boldsymbol{R}_2,a_1,a_2} J^K_{\boldsymbol{R},\boldsymbol{R}_1 a_1,\boldsymbol{R}_2 a_2}\left[N\zeta_{\boldsymbol{R},\boldsymbol{R}_2 a_2}\zeta^*_{\boldsymbol{R},\boldsymbol{R}_1 a_1} - \sum_\sigma\left(\zeta^*_{\boldsymbol{R},\boldsymbol{R}_1 a_1} f^\dagger_{\boldsymbol{R},\sigma} c_{\boldsymbol{R}_2,a_2,\sigma} + \eta_{\boldsymbol{R},\boldsymbol{R}_2 a_2} c^\dagger_{\boldsymbol{R}_1,a_1,\sigma} f_{\boldsymbol{R},\sigma}\right)\right] \\
H_{Hund} &\to \sum_{\boldsymbol{R},a}\frac{J_a}{2}\left[-N\zeta_{\boldsymbol{R},\boldsymbol{R}a}\zeta^*_{\boldsymbol{R},\boldsymbol{R}a} + \sum_\sigma\left(\zeta^*_{\boldsymbol{R},\boldsymbol{R}a} f^\dagger_{\boldsymbol{R},\sigma} c_{\boldsymbol{R},a,\sigma} + \text{h.c.}\right)\right],
\end{aligned}
\tag{S9}
$$

where $\chi_{\boldsymbol{R},\boldsymbol{R}'}, \eta_{\boldsymbol{R},\boldsymbol{R}_1 a_1}$ are the bosonic fields used in the decoupling procedure. The large N limit leads to saddle point equations

$$
\begin{aligned}
\chi_{\boldsymbol{R},\boldsymbol{R}'} &= \frac{1}{N}\sum_\sigma \langle f^\dagger_{\boldsymbol{R},\sigma} f_{\boldsymbol{R}',\sigma}\rangle\,, \\
\zeta_{\boldsymbol{R},\boldsymbol{R}'a} &= \frac{1}{N}\sum_\sigma \langle f^\dagger_{\boldsymbol{R},\sigma} c_{\boldsymbol{R}',a,\sigma}\rangle\,.
\end{aligned}
\tag{S10}
$$

The local constraints $\sum_\sigma f^\dagger_{\boldsymbol{R},\sigma} f_{\boldsymbol{R},\sigma} = 1$ are satisfied on average by introducing a Lagrangian multiplier λ: $\lambda(\sum_\sigma f^\dagger_{\boldsymbol{R},\sigma} f_{\boldsymbol{R},\sigma} - 1)$. At the saddle point, λ is determined by requiring

$$
\sum_\sigma \langle f^\dagger_{\boldsymbol{R},\sigma} f_{\boldsymbol{R},\sigma}\rangle = 1 \tag{S11}
$$

We solve Eqs. S10 and S11 self-consistently and derive the phase diagram at zero temperature as shown in the main text. In the small Fermi-surface phase, the Luttinger theorem of the Kondo lattice is seen as satisfied by the separate responses of the local moments and conduction electrons (*8, 44*) to the adiabatic insertion of an external flux (*45*).

G. Symmetry properties in the heavy fermion phase

In the heavy Fermi liquid phase, $\hat{\varsigma}_{\boldsymbol{R},\boldsymbol{R}',a}$ condensates. The condensation locks the phase factors of the pseudo-fermion under the $U(1)$ gauge and M_x mirror transformations to those of the physical c-electrons. Thus, $f_{\boldsymbol{R},\sigma}$ acquires not only a $U(1)$ physical charge as in the standard Kondo model, but also the $+1$ mirror eigenvalue. Thus the heavy bands induced by the Kondo effect has $+1$ mirror eigenvalue along Γ-K lines. Consequently, its crossing with wide bands of -1 mirror eigenvalue is symmetry-protected.

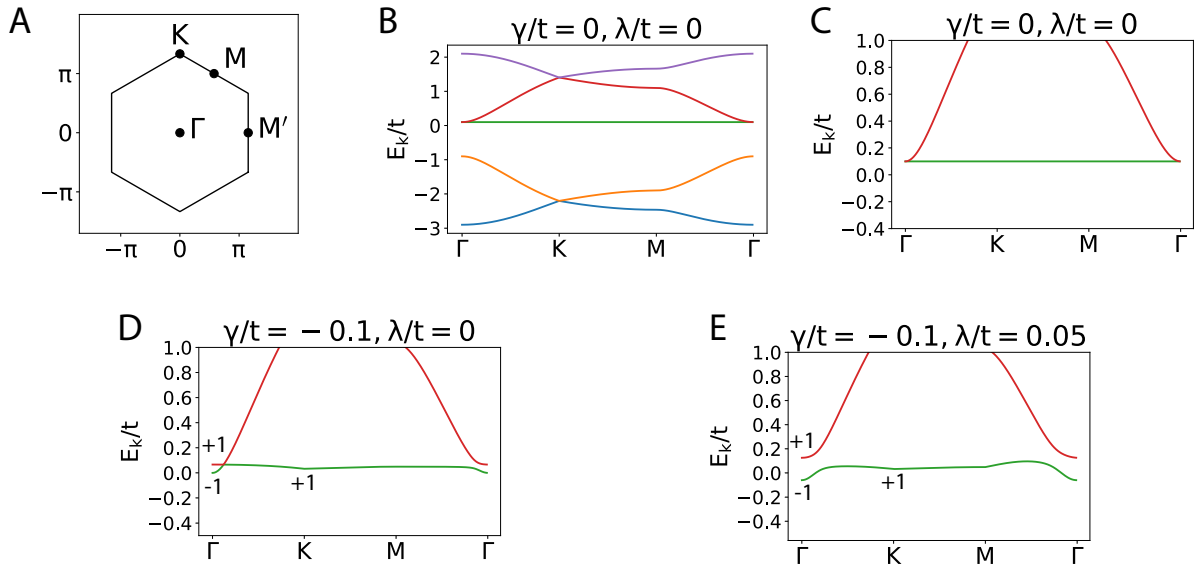

Figure S1: **Brillouin zone and the noninteracting bandstructure.** The first Brillouin zone (**A**). Full band structure (**B**) and zoomed-in band structure (**C**) at $\gamma = \lambda = 0$ with a completely flat band near the Fermi energy. (**D**) Band structure at non-zero γ and $\lambda = 0$. We observe a relatively flat band and a Dirac node between the flat and wide bands. (**E**) Band structure at a non-zero γ and a non-zero λ, the Dirac node is gapped by the spin-orbit coupling and the flat band acquires ± 1 Chern number. In (**D**) and (**E**), we label the M_x eigenvalues of the relevant bands at the high symmetry points.

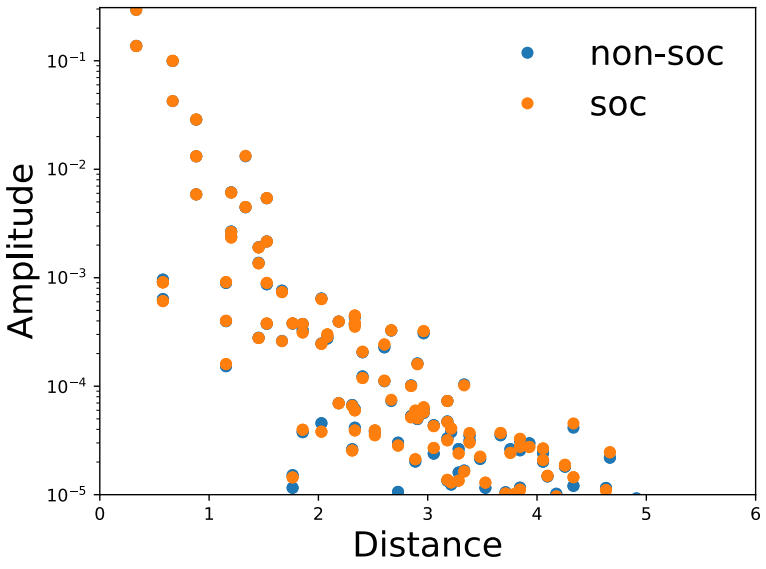

Figure S2: **Decaying of the wavefunction amplitudes of the Wannier function.** The Wannier functions of the d electrons (with non-zero SOC and zero SOC) decay exponentially. The decaying of the two cases is similar with only a small deviation at long distances, since the two Wannier orbitals are adiabatically connected with each other.

Momentum	Γ	M'	K
M_x eigenvalue of band 1	+1	-1	+1
M_x eigenvalue of band 2	+1	+1	-1
M_x eigenvalue of band 3	-1	+1	+1

Table S1: M_x symmetry eigenvalues of the top three bands. We label the bands from the top to the bottom as 1,2,3,4,5.

(i,j)	$(0,1)$	$(-1,0)$	$(1,0)$	$(0,-1)$	$\pm(-2,2)$	$(-2,0)$	$(0,2)$	
$t^d_{ia_1+ja_2}/t$	-0.023	-0.023	-0.023	-0.023	0.025	0.019	0.019	
	$(2,0)$	$(0,-2)$	$\pm(-1,2)$	$\pm(2,-1)$	$\pm(-1,1)$			
	0.019	0.019	-0.017	-0.017	0.01			
(i,j)	$(1,0)$	$(0,-1)$	$(1,1)$	$(-1,-1)$	$(-1,2)$	$(-2,1)$	$(1,-2)$	$(2,-1)$
$V_{ia_1+ja_2,1}/t$	0.066	-0.066	-0.025	0.025	0.047	-0.047	0.040	-0.040
	$(2,0)$	$(0-2)$	$(-3,2)$	$(-2,3)$	$(1,1)$	$(-1,-1)$		
	0.032	-0.032	-0.028	0.028	-0.025	0.0205		
(i,j)	(0,0)	$(0,1)$	$(-1,0)$	$(1,0)$	$(0,-1)$	$(1,-1)$	$(-1,1)$	
$V_{ia_1+ja_2,2}/t$	-0.04	0.0481	0.0481	0.0457	0.0457	-0.0758	-0.0726	
	$(1,1)$	$(-1,-1)$	$(2,-2)$	$(-1,2)$	$(-2,1)$	$(2,0)$	$(0,-2)$	$(-2,2)$
	-0.0377	-0.0377	0.0384	0.0365	0.0365	0.0275	0.0275	-0.0242
(i,j)	$(0,1)$	$(0,-1)$	$(-1,0)$	$(1,0)$	$(-1,1)$	$(1,-1)$	$(-1,-1)$	$(1,1)$
$t^c_{ia_1+ja_2,11}$	-0.1768	-0.1768	-0.1768	-0.1768	-0.0789	-0.0789	-0.0378	-0.0378
	$(2,-2)$	$(-2,2)$						
	-0.0403	-0.0403						
(i,j)	$(0,-1)$	$(0,1)$	$(-1,0)$	$(1,0)$	$(-1,-1)$	$(1,1)$	$(2,0)$	$(-2,0)$
$t^c_{ia_1+ja_2,22}$	0.1389	0.1389	0.1389	0.1389	0.0292	0.0292	-0.0383	-0.0383
	$(0,-2)$	$(0,2)$						
	-0.0383	-0.0383						
(i,j)	$(0,-1)$	$(0,1)$	$(-1,0)$	$(1,0)$	$(1,-2)$	$(2,-1)$	$(-1,2)$	$(-2,1)$
$t^c_{ia_1+ja_2,12}$	0.218	0.076	-0.076	-0.218	0.098	-0.098	0.046	-0.046
	$(2,-3)$	$(3,-2)$	$(3,-4)$	$(4,-3)$	$(3,0)$	$(0,-3)$		
	0.058	-0.058	0.029	0.029	-0.022	0.022		
	E_d/t	E_1/t	E_2/t					
	-0.01	0.91	1.36					

Table S2: Parameters of the kinetic term in the Wannier basis (here we only show the term with absolute value lager than 0.02).